


Angular-momentum coupling of optical whispering-gallery modes to liquid droplet microresonatorsDavide D'Ambrosio ^{1,*}, Xavier Zambrana-Puyalto ^{1,2}, Marialuisa Capezzuto,¹ Antonio Giorgini,¹ Pietro Malara,¹ Saverio Avino,¹ and Gianluca Gagliardi¹¹*Consiglio Nazionale delle Ricerche, Istituto Nazionale di Ottica (INO), via Campi Flegrei 34, Comprensorio A. Olivetti, I-80078 Pozzuoli, Italy*²*Istituto Italiano di Tecnologia, Via Morego 30, 16136 Genova, Italy*

(Received 9 August 2021; accepted 14 September 2021; published 7 October 2021)

Starting from a recently developed model based on the generalized Lorenz-Mie theory, we simulate and experimentally investigate the resonance spectrum and the scattered light field of whispering-gallery modes (WGMs) in a liquid droplet excited with a free-space visible laser beam. Depending on the illumination configuration and the spectral region, we observe WGMs with diverse quality factors and coupling efficiencies. Through imaging of scattering patterns, we show a robust agreement between theory and experiment. Our study provides an insight of the free-space optical coupling phenomenon, opening pathways for a controlled excitation of ultrahigh-quality WGMs in a plethora of liquid and solid optical microresonators for sensing and imaging applications.

DOI: [10.1103/PhysRevA.104.043504](https://doi.org/10.1103/PhysRevA.104.043504)**I. INTRODUCTION**

Optical resonances in spheroidal, cylindrical, ringlike, and toroidal structures were historically termed morphology-dependent resonances (MDRs) because of their dependence on the specific geometry of the dielectric host structure [1,2]. The popular analogy with acoustic whispering-gallery modes (WGMs) takes its name from the sound waves guided by closed curved galleries, first studied by Lord Rayleigh [1], nowadays observed in several structures all over the world. In the optical domain, WGMs are a subclass of MDRs that exhibit high-quality factors (Q factors) and shallow nature. Indeed, in WGMs, light circulates along equatorial trajectories close to the surface before it is scattered or absorbed. With an appropriate choice of material and wavelength, narrow resonances with Q factors in excess of 10^9 can be observed in the visible and near-infrared spectral regions [3]. Although in most of the literature WGMs are excited via frustrated total internal reflection in tapered optical fibers and prisms [4], direct coupling of free-space laser beams to axially symmetric microspheres was originally proposed in seminal works on aerosols in the 1980s–90s [5,6]. However, in most previous works, the MDRs were associated with low- Q elastic-scattering resonances collectively observed in micrometer-sized particles falling from a fast-vibrating orifice [6]. In this framework, theoretical models based on Lorenz-Mie scattering were developed to explain the resonant features and the coupling mechanism [7,8]. In these works, the free-space coupling process is assumed to originate from the surface imperfections and deviations from a perfect spherical geometry, which leads to an optical angular-momentum (AM) transfer phenomenon as a result of violation of Van de Hulst's

localization principle [8]. Also, these models were based on the plane-wave decomposition of a paraxial beam; thus, they could not capture all the subtleties of tightly focused beam illumination. On the other hand, over the last few years, few direct free-space coupling and interrogation schemes have been experimentally demonstrated for single, free-standing active [9], and passive droplets with up to millimeter size, showing the ability to use them as optically resonant sensors [10,11].

In a recent work, we have theoretically described the physics behind free-space coupling of a light beam to the WGMs of a spherical microresonator even in the absence of superficial scattering sites or deformations [12]. Our semi-analytical model is based on symmetries, which presents two main advantages: (i) insights can be drawn from the model without using complex mathematical formulas; and (ii) it uses very efficiently the computation resources thus allowing for exact electromagnetic calculations for very large particles (300 μm and above). Here, we investigate the resonant scattering of a pendant liquid droplet illuminated by a tangential free-space laser beam. We compare the direct experimental observations with the theoretical predictions of a model drawn for a perfectly spherical resonator based on the above-described formalism [13]. Our model shows that free-space tangential illumination of a spherical resonator allows for the selective excitation of WGM resonances with diverse quality factors. Depending on their Q -factor value, WGMs are expected to produce different circular patterns for the scattered intensity. We experimentally confirm these predictions by exciting droplet microresonators with direct laser light in various alignment conditions and imaging the scattered intensity on a camera. Last but not least, we predict the coupling efficiency of a free-space laser beam into a particular WGM as a function of the transverse distance and validate it experimentally.

*davide.dambrosio@ino.cnr.it

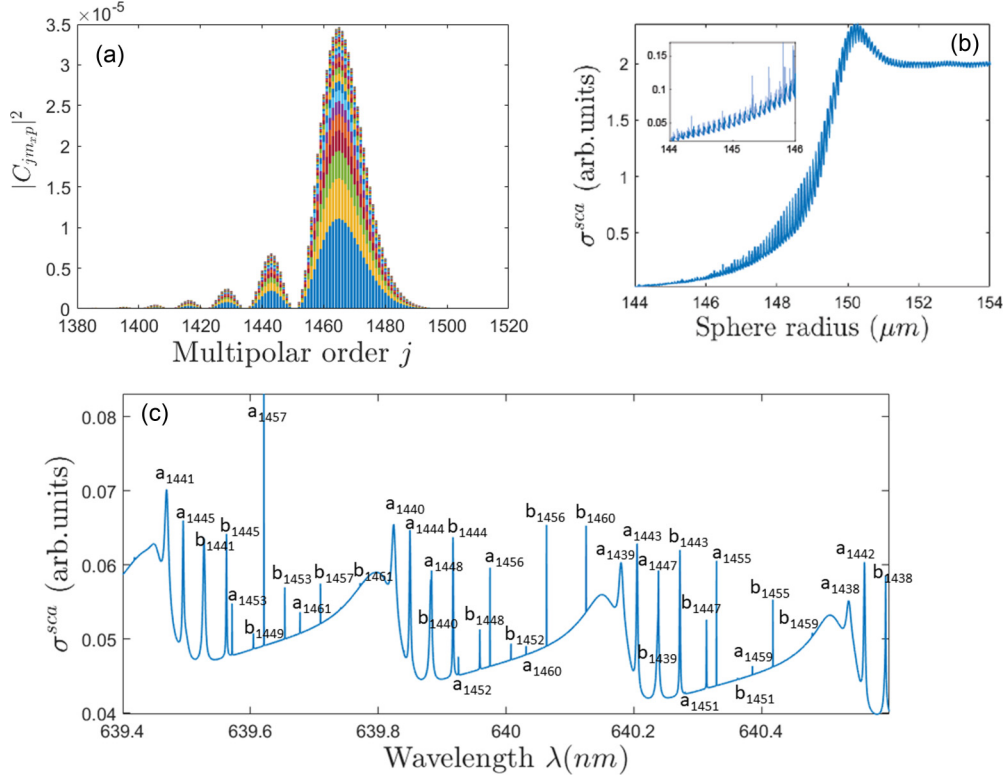


FIG. 1. (a) Multipolar decomposition of a circularly polarized Gaussian beam displaced by $d = 150 \mu\text{m}$ along the y direction, focused by a lens with $\text{NA} = 0.4$, and for $\lambda = 640 \text{ nm}$. Different colors indicate the weights of modes corresponding to different m_x values (blue for $m_x = j$, yellow for $m_x = j-1$, etc.). (b) Normalized scattering cross section σ^{sca} calculated for the same beam interacting with a particle of radius R with $n_r = 1.3989$. The inset shows a zoom in the range $R = 144\text{--}146 \mu\text{m}$. (c) Resonance spectrum of a sphere with $R = 145 \mu\text{m}$ and $n_r = 1.3989$, excited with the same beam as in (a) (displaced by $d = 150 \mu\text{m}$) and calculated over a 1.2-nm wavelength interval.

II. THEORETICAL FRAMEWORK

Let us consider a spherical dielectric microresonator with radius R and a refractive index n_r relative to a uniform surrounding medium. The center of the sphere coincides with the center of our reference frame, with the z axis being the propagation direction of a Gaussian beam (for further details refer to Sec. III). Following the approach of Ref. [12] in a generalized Lorenz-Mie theory framework [13], we first calculate the multipolar decomposition of a Gaussian beam with a displacement d along the y direction. The multipolar fields $\{\mathbf{A}_{jm}^{(e)}, \mathbf{A}_{jm}^{(m)}\}$ are a basis of solutions of Maxwell equations, and any incoming beam \mathbf{E}^{in} can be decomposed into them: $\mathbf{E}^{\text{in}} = \sum_{j,m} g_{jm}^{(e)} \mathbf{A}_{jm}^{(e)} + g_{jm}^{(m)} \mathbf{A}_{jm}^{(m)}$, with $\{g_{jm}^{(e)}, g_{jm}^{(m)}\}$ being the beam-shape coefficients [13]. When the incoming beam \mathbf{E}^{in} is an eigenstate with eigenvalue p of the helicity operator Λ [14–16], then the two beam-shape coefficients collapse into a beam-shape function C_{jmp} : $\mathbf{E}^{\text{in}} = \sum_{j,m} C_{jmp} (\mathbf{A}_{jm}^{(e)} + ip \mathbf{A}_{jm}^{(m)})$ [14–16]. The knowledge of the beam-shape function C_{jmp} analytically solves the Mie scattering problem, as the scattered field is expressed as a function of it. Note that m corresponds to the value of the projection of the angular momentum (AM) of the multipolar fields onto a certain axis. In this work, we are interested in the WGMs that revolve around the x axis (see Fig. 5); therefore, we will choose $m = m_x$. In Fig. 1(a), we show the multipolar decomposition (i.e., we display the beam-shape function $C_{j m_x p}$) of a circularly polarized Gaussian beam displaced a distance $d = 150 \mu\text{m}$ along the y axis. The

beam is focused with a microscope objective with numerical aperture (NA) = 0.4, and it has a wavelength of $\lambda = 640 \text{ nm}$. The formula to compute $C_{j m_x p}$ has been given in our previous work [12] and it reads as follows:

$$C_{j, m_x, p}^{\text{off}, d\hat{y}} = \sum_{n = -\min(j, j')}^{\min(j, j')} \sum_{L=0}^{\infty} (2L+1) (-i)^L j_L(kd) \times \langle j, n; L, 0 | j', n \rangle \langle j, p; L, 0 | j', p \rangle \sum_{j' = m_z^*}^{\infty} \sum_{m_z = -j}^j d^j (-\pi/2)_{m_z}^{m_x} D^j(\hat{d})_n^{m_z} D^{j'}(\hat{d})_n^{m_z^*} C_{j', m_z^*, p}^{\text{on}}$$

where $C_{j m_x p}^{\text{on}}$ is the beam-shape function $C_{j m_x p}$ of the same circularly polarized Gaussian beam when $d = 0$. Its analytical expression can be found in Ref. [16]. Note that the x axis of Fig. 1(a) shows the multipolar values j in between 1380 and 1520. All the rest of multipolar values from 1 to 1379 and from 1521 to infinity are not given because they are negligible. Indeed, our theoretical model predicts that any cylindrically symmetric beam with a certain displacement allows for the excitation of a WGM of order j^* (proportional to d) in a spherical structure illuminated by it. In this particular case with $d = 150 \mu\text{m}$, j^* ends up being in the range of $j^* = [1400, 1500]$ [see Fig. 1(a)]. Furthermore, all that has a fundamental physical meaning: the displacement of a Gaussian beam from the center plays the same role as an intrinsic angular momentum.

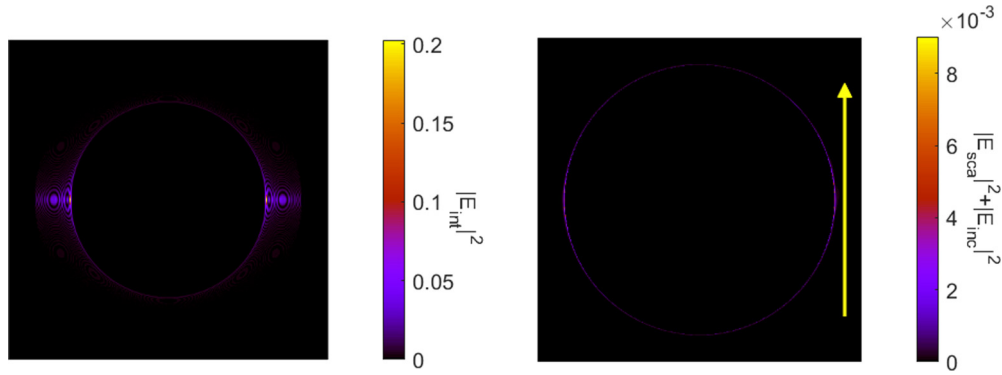


FIG. 2. Square modulus of the electric field for the internal field (left panel), for the incident field (along yellow arrow direction), and for the scattered field (right panel). The incident intensity, barely visible, is that of a circularly polarized Gaussian beam at 640.063295 nm focused with a $\text{NA} = 0.4$ at a distance $d = 150 \mu\text{m}$ from the center of the sphere along the y direction. The wavelength has been chosen to excite the WGM given by b_{1456} .

However, this angular momentum is distributed among a variety of multipolar modes. Hence, with tangential scattering of a free-space Gaussian beam, it is impossible to excite a single WGM with *ideal* critical coupling [3].

Using the multipolar decomposition given above for $d = 150 \mu\text{m}$, we calculated the scattering cross section as a function of the microresonator radius [see Fig. 1(b)], paying particular attention to the interval across $R/d \cong 1$ (inset), with R varying between 144 and $150 \mu\text{m}$. In this parameter region, which corresponds to a tangential illumination, the system exhibits several sharp resonances, as shown in the inset of Fig. 1(b). That is because an efficient excitation of WGMs requires that $R/d < 1$ but very close to 1 [12]. In Fig. 1(c) we also show the spectrum of a spherical microresonator with $R = 145 \mu\text{m}$ and $n_r = 1.3989$, around 640 nm. It can be noticed that the optical resonances repeat with a free-spectral range periodicity, but with slightly different relative intensities. We label them as a_j and b_j , where the index j is directly related to the multipolar order of the mode, and a/b refer to the electric (magnetic) parity of the modes that can be expressed in terms of their polarization [12]. However, in the simulation, we assumed an incident beam with circular polarization in order to consider both electric and magnetic mode types.

An example of the light-field spatial distribution of a WGM is shown in Fig. 2. The internal electric-field square modulus is displayed on the left, while the incident + scattered fields are on the right. We plotted them in two separate panels because of their large intensity difference. For these calculations, the wavelength was set to $\lambda = 640.063295$ nm, corresponding to the sharp resonance given by the b_{1456} coefficient [Fig. 1(c)]. In our experiment, we mainly worked with microresonators having $R \approx 150 \mu\text{m}$. However, in the simulation, we reduced the droplet radius to $R = 62 \mu\text{m}$ in order to increase the image resolution while maintaining a reasonable computation time without loss of generality. In this way, the simulated scattered field shows a regular distribution and two brighter spots at the poles (Fig. 3, left panel), as also observed in past works with conventional coupling schemes [17,18].

In Fig. 3, right panel, a natural logarithmic plot improves the visibility of the fast-fading external electric field: a counterclockwise WGM gives rise to a spiral pattern, with several minima and maxima, thus suggesting a large AM content of the circulating beam.

Up until this point, only the fields of very sharp resonances have been simulated. In Fig. 4, instead, we show the simulated resonance spectrum and the intensity scattered by the

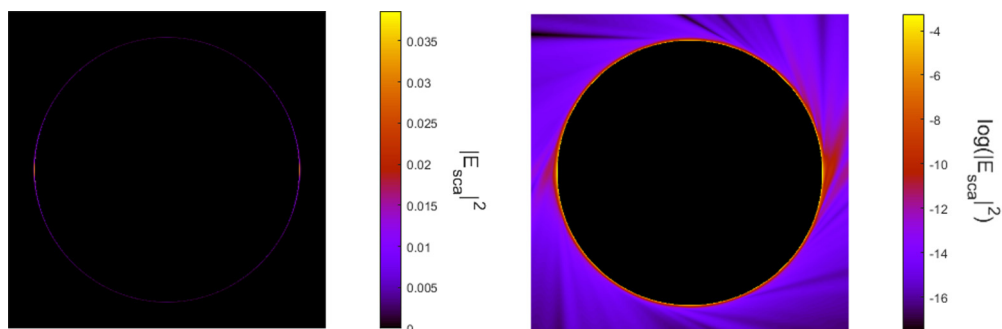


FIG. 3. On the left is a $150 \times 150\text{-}\mu\text{m}^2$ window showing the squared modulus of the scattered electric field of a microresonator with $R = 62 \mu\text{m}$ and $n_r = 1.45$ illuminated by a circularly polarized Gaussian beam displaced by $d = 64 \mu\text{m}$ from the center and focused with a lens of $\text{NA} = 0.4$. On the right, the natural logarithm of the left plot is also shown. The resonant wavelength for these simulations is $\lambda = 639.99111$ nm.

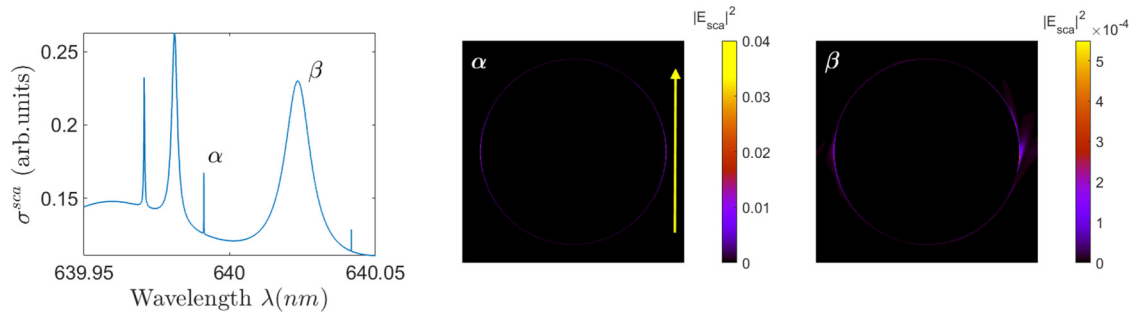


FIG. 4. Simulated resonance spectrum (on the left) and scattered field distributions of α and β WGMs (central and right panel, respectively) for a microresonator with $R = 62 \mu\text{m}$ and $n_r = 1.45$. The incident radiation is circularly polarized, propagating along the z direction (yellow arrow), and has been focused by a lens with $\text{NA} = 0.4$. In the last panel, β ($\lambda_\beta = 640.0234 \text{ nm}$) corresponds to a low- Q mode, which exhibits high losses slightly visible as directional emission from the surface. Moving to the higher- Q mode α ($\lambda_\alpha = 639.97067 \text{ nm}$) losses are gradually reduced and the intensity of the scattered light is about two orders of magnitude larger.

microresonator when WGMs with very different quality factors are excited. Here, the spiral pattern of the low- Q factors modes (e.g., WGM β) is only barely visible, while sharper resonances (e.g., WGM α) exhibit nearly zero radial losses and scattered intensity higher by up to two orders of magnitude (see scale bars in Fig. 4).

III. EXPERIMENT VALIDATION AND COMPARISON

The outcome of our simulations was compared with a laboratory experiment on free-space excitation of a pendant droplet with diameter D . A sketch of the experimental setup is depicted in Fig. 5. The light beam from a distributed-feedback diode laser operating at 640 nm (8-mW power) was tightly focused with an $\text{NA} = 0.4$ at the surface of a silicone-oil (XIAMETER™ PMX-200 10 cSt) droplet with $n_r = 1.3989$. The droplet is suspended by a vertical optical fiber along its axis under the action of gravity and interfacial forces. Basically, the droplet may be approximated as a prolate spheroid with an eccentricity ε defined as the normalized difference

between polar and equatorial radii [10]. Given the Bond number of our droplets $B = (D/l_c)^2 < 1$ ($l_c = \sqrt{\frac{\sigma}{\rho g}}$, where σ and ρ are the liquid surface tension and density, respectively), the interfacial forces dominate over gravity and the droplet remains attached to the fiber tip with minimal deformation. In this condition, we can treat the droplet as an almost perfect spherical microresonator with $\varepsilon < 10^{-3}$. This is confirmed by the fact that we did not observe any mode-degeneracy lift in our scattering and transmission spectra [19]. Also, the optical losses due to absorption by silicone oil were neglected since they mostly limit the maximum achievable Q factor [20] while they affect our scattering simulation only to a minor extent.

We acquired the resonance spectra from the transmitted and backscattered light with Si photodetectors. In particular, the backscattered beam, which is recollimated through the focusing objective, is collected behind the laser on a separate photodetector [20]. Light outscattered from the droplet surface is collected with a 45° silver mirror and imaged on a charge-coupled device (CCD) camera through a $4f$ lens system. In Fig. 6(a) we show an image of the droplet in nitrogen-enriched atmosphere, lit up by the laser beam effectively intersecting the droplet surface. For $R/d > 1$, only

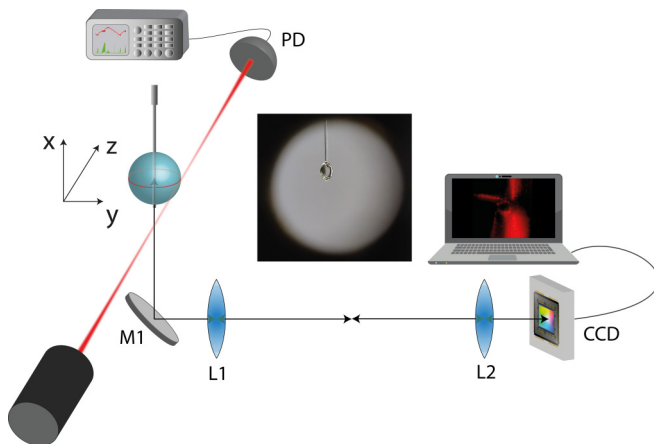


FIG. 5. A pendant droplet of silicone oil (shown in the photo) is tangentially excited by a Gaussian beam and the light scattered from the microresonator surface is collected underneath by a 45° silver mirror (M1). The signal passes through a $4f$ lens system (L1 and L2) and is focused onto a CCD camera. The wavelength of the laser is 640.0 nm .

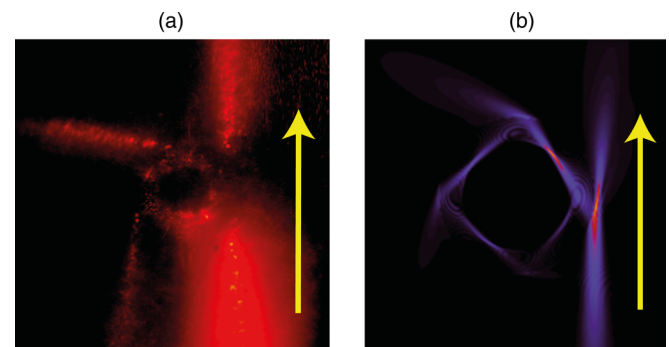


FIG. 6. (a) An image of the light scattered by a droplet microresonator when $R/d > 1$. In this alignment condition, the laser beam propagating along the yellow arrow direction intersects the resonator surface. The image has been taken in a nitrogen-enriched atmosphere to highlight the directional emission pattern of the resonator surface. In panel (b) a simulation corresponding to a spherical microresonator is given for the same alignment condition.

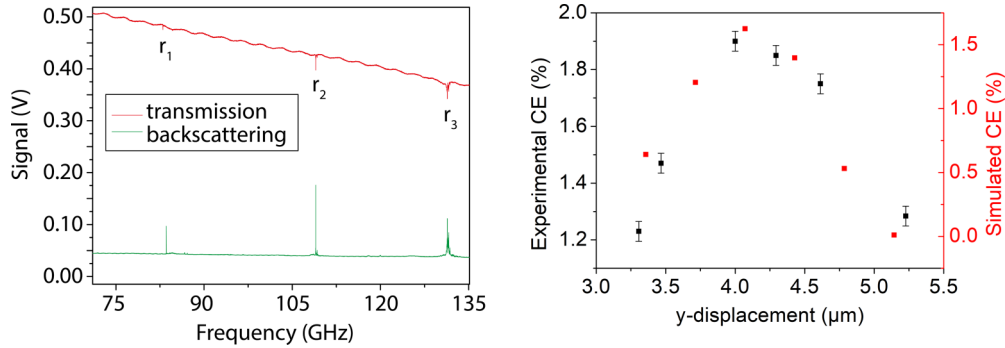


FIG. 7. In the left panel the resonance spectrum of a droplet with $R = 156.5 \mu\text{m}$ shows WGMs with different widths and intensities, likely corresponding to b modes with $j \sim 1452\text{--}1460$. On the right, a comparison between the measured CE and simulated CE (b_{1456} coefficient) as a function of the beam tangential relative displacement.

broad MDRs can be excited: this leads to the peculiar directional emission pattern observed in the scattering image, in agreement with the simulation [Fig. 6(b)].

Then, we increased the displacement d to achieve the condition with R/d slightly less than 1 and excite high- Q WGMs. Indeed, our simulations [Fig. 1(c)] clearly indicate that, in this alignment condition, the WGM spectrum is populated by several resonances with different Q factors. Accordingly, in Fig. 7, left panel, we give a spectrum with three different WGMs of a microresonator having $R = 156.5 \mu\text{m}$. We note that the excitation laser is linearly polarized in the incidence (horizontal) plane, which implies that this spectrum lacks some modes if compared with the theoretical one in Fig. 4, where the polarization state was set circular to observe all possible WGMs (a and b symmetries).

Let us now define the coupling efficiency (CE) as the ratio between the optical power that is effectively coupled within the microresonator on the WGM peak and the total incident optical power. The condition $\text{CE} = 1$ corresponds to critical

coupling to the microresonator [3]. In Fig. 7, right panel, we compare the CE measured for r_1 (see left panel) and that simulated for a high- Q mode corresponding to the b_{1456} coefficient. From this plot, it is worth noting the fair agreement of experimental data with predictions. Besides, we observe that both the experimental and theoretical CE is on the order of 2%. Note that this measurement provides a good qualitative estimate of the CE trend with beam-droplet displacement and is clearly within the boundaries calculated in a previous work [20]. For different WGMs, we observed a significantly larger CE, up to 10% for resonances with larger linewidths.

The experimental scattered-light patterns of the most intense modes r_2 and r_3 are shown in Fig. 8. On top of the spurious spots due to the scattering of focusing and collection objectives, two circular patterns are immediately recognizable on each image: the bright, thin external ring near the liquid interface corresponds to the excited WGM and, in fact, it perfectly matches the prediction of our simulation. The smaller ring, internal to the surface, is instead given by light symmetrically scattered by the fiber that sits on the vertical axis of the droplet and holds it suspended, as confirmed by recordings of Figure 1s(a) and Figure 1s(b) (Supplemental Material [21]).

Harnessing the photothermal and radiation pressure effects of high- Q microresonators, it is possible to achieve a stable resonant condition. Indeed, owing to the cavity expansion, the resonance tends to spontaneously lock in close proximity of the laser frequency [22,23]. In this condition, the transmitted and scattered laser power keeps an almost constant level, as shown in Fig. 8, upper right panel. This phenomenon is clearly illustrated by the video V1 of the Supplemental Material, where laser locking spontaneously occurs and the droplet outer ring changes its state from off to on. In the last two panels of Fig. 8, the scattered light distribution is shown for each WGM. As expected from our simulations, the light rings of modes with different Q factors exhibit the very same pattern but different intensities. This effect is also shown in video V2, where the passage through resonance is seen when the laser is swept through WGMs.

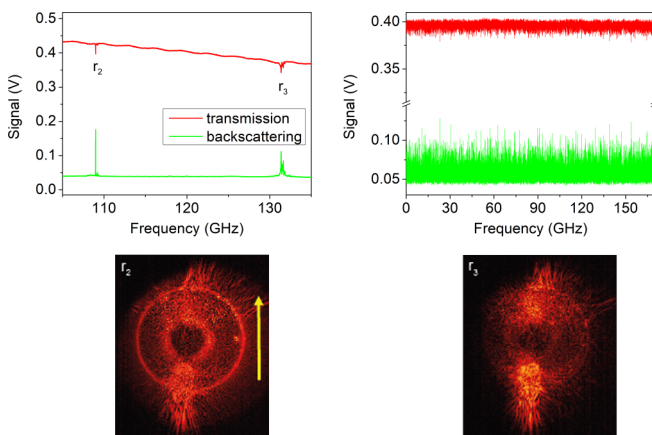


FIG. 8. Two whispering-gallery modes of a liquid microresonator ($R = 156.5 \mu\text{m}$) are compared. The upper left panel shows the resonance spectrum of a WGM microresonator excited by a free-space laser beam propagating along the z direction (yellow arrow). In the upper right panel, the red and green traces show the same recording acquired in cavity self-locking condition for the backscattered and transmitted signals (no scan). The ring pattern is bright and clearly recognizable when a high- Q factor mode is excited (r_2), whereas it is barely visible for lower- Q factor modes (r_3).

IV. CONCLUSION

On the basis of a previously developed analytical model [12], we simulated the scattering cross section and the optical resonance spectrum of a spherical microresonator under

free-space illumination. In particular, the model describes the excitation configurations of WGMs as a function of the distance between the beam and the microresonator. We validated our simulations through direct imaging and spectroscopy of vertically suspended liquid droplets made of silicone oil. We compared the experimental results with our theoretical predictions finding a very good agreement for the WGM resonance spectral features, their coupling efficiencies, and scattered light patterns for specific alignment conditions. This confirms that our model enables a quantitative study of different optical scattering-based excitation regimes to design high- Q microresonators in a robust scheme. Also, we proved that for free-space coupled microcavities, the bare collection of light scattered from the surface is a reliable readout, capable of distinguishing between different WGMs.

Understanding such mechanisms allows avoiding complex and short-lasting coupling and collecting equipment (e.g., tapered fibers and waveguides) widening the application range of such sensors in practical procedures. Furthermore, a full control of WGMs would lead to their selective excitation

with optimized coupling efficiency and surface localization. This paves the way to a platform of solid and liquid microresonators that lends itself to nanophotonic sensing and hyperspectral imaging.

ACKNOWLEDGMENTS

The authors are grateful to Marco Conti, Andrea Passarella, and Claudio Cicconetti for the availability of the CNR-IIT high-performance computer facility. The authors are grateful to G. Notariale for technical assistance. X.Z-P. acknowledges funding from the European Union's Horizon 2020 research and innovation programme under the Marie Skłodowska-Curie Grant Agreement No. 795838. The experimental work and Davide D'Ambrosio's fellowship were funded by the Italian Ministry for University & Research (MUR) in the framework of the PRIN2017 PELM project (20177PSCKT grant).

-
- [1] L. Rayleigh, *Philos. Mag.* **20**, 1001 (1910).
 - [2] S. C. Hill and R. E. Benner, *J. Opt. Soc. Am.* **3**, 1509 (1986).
 - [3] A. B. Matsko and V. S. Ilchenko, *IEEE J. Sel. Top. Quantum Electron.* **12**, 3 (2006).
 - [4] A. B. Matsko and V. S. Ilchenko, *IEEE J. Sel. Top. Quantum Electron.* **12**, 15 (2006).
 - [5] R. E. Benner, P. W. Barber, J. F. Owen, and R. K. Chang, *Phys. Rev. Lett.* **44**, 475 (1980).
 - [6] H. B. Lin, J. D. Eversole, and A. J. Campillo, *Rev. Sci. Instrum.* **61**, 1018 (1990).
 - [7] E. E. Khaled, S. C. Hill, and P. W. Barber, *IEEE Trans. Antennas Propag.* **41**, 295 (1993).
 - [8] H. B. Lin, J. D. Eversole, A. J. Campillo, and J. P. Barton, *Opt. Lett.* **23**, 1921 (1998).
 - [9] A. Kiraz, A. Kurt, M. A. Dündar, M. Y. Yüce, and A. L. Demirel, *J. Opt. Soc. Am. B* **24**, 1824 (2007).
 - [10] S. Avino, A. Krause, R. Zullo, A. Giorgini, P. Malara, P. De Natale, H. P. Looock, and G. Gagliardi, *Adv. Opt. Mater.* **2**, 1155 (2014).
 - [11] A. Giorgini, S. Avino, P. Malara, P. De Natale, and G. Gagliardi, *Sensors* **19**, 473 (2019).
 - [12] X. Zambrana-Puyalto, D. D'Ambrosio, and G. Gagliardi, *Laser Photonics Rev.* **15**, 2000528 (2021).
 - [13] G. Gouesbet and G. Gréhan, *Generalized Lorenz-Mie Theories* (Springer, Berlin, Heidelberg, Germany, 2011).
 - [14] X. Zambrana-Puyalto, X. Vidal, and G. Molina-Terriza, *Opt. Express* **20**, 24536 (2012).
 - [15] X. Zambrana-Puyalto, X. Vidal, P. Woźniak, P. Banzer, and G. Molina-Terriza, *ACS Photonics* **5**, 2936 (2018).
 - [16] X. Zambrana-Puyalto, Ph.D. thesis, Macquarie University, Sydney, NSW, Australia, 2014.
 - [17] J. Dominguez-Juarez, G. Kozyreff, and J. Martorell, *Nat. Commun.* **2**, 254 (2011).
 - [18] S. A. Anand, M. A. Eryürek, Y. B. Karadag, A. A. Erten, A. A. Serpengüzel, A. C. Jonás, and A. Kiraz, *J. Opt. Soc. Am. B* **33**, 1349 (2016).
 - [19] H. M. Lai, P. T. Leung, K. Young, P. W. Barber, and S. C. Hill, *Phys. Rev. A* **41**, 5187 (1990).
 - [20] A. Giorgini, S. Avino, P. Malara, P. De Natale, and G. Gagliardi, *Sci. Rep.* **7**, 41997 (2017).
 - [21] See Supplemental Material at <http://link.aps.org/supplemental/10.1103/PhysRevA.104.043504> for scattered light patterns and videos.
 - [22] V. B. Braginsky, M. L. Gorodetsky, and V. S. Ilchenko, *Phys. Lett.* **137**, 393 (1989).
 - [23] A. Giorgini, S. Avino, P. Malara, P. De Natale, M. Yannai, T. Carmon, and G. Gagliardi, *Phys. Rev. Lett.* **120**, 073902 (2018).